Understanding tunneling magnetoresistance during thermal annealing in MgO-based junctions with CoFeB electrodes

W. G. Wang,[1,*] C. Ni,[2] G. X. Miao,[3] C. Weiland,[2] L. R. Shah,[1] X. Fan,[1] P. Parson,[1] J. Jordan-sweet,[4] X. M. Kou,[1] Y. P. Zhang,[1] R. Stearrett,[1] E. R. Nowak,[1] R. Opila,[2] J. S. Moodera,[3] and J. Q. Xiao[1,†]

[1]*Department of Physics and Astronomy, University of Delaware, Newark, Delaware 19716, USA*

[2]*Department of Materials Science and Engineering, University of Delaware, Newark, Delaware 19716, USA*

[3]*Francis Bitter Magnet Laboratory, MIT, Cambridge, Massachusetts 02139, USA*

[4]*IBM T.J. Watson Research Center, Yorktown Heights, New York 10598, USA*

(Received 24 November 2009; revised manuscript received 16 March 2010; published 7 April 2010)

The competition between the interface crystallization and diffusion processes, their influence on the onset of symmetry-filtering coherent tunneling of Δ_1 band electrons in the MgO-based magnetic tunnel junctions is investigated. Systematic study of the transport and magnetoresistance during thermal annealing of these junctions shows a unique behavior of the tunneling conductance in the parallel state. The optimal annealing time for achieving giant tunneling magnetoresistance at different temperatures is determined. The evolution of magnetoresistance consists of three distinct regions, responsible by different contributions from CoFeB electrodes and the MgO barrier. The whole phenomenon can be understood through an empirical model based on the Landauer tunneling picture.

DOI: 10.1103/PhysRevB.81.144406 PACS number(s): 72.25.−b, 73.43.Qt, 85.70.Kh, 73.40.Gk

The transmission probability of the Bloch electrons in an epitaxial ferromagnet/insulator/ferromagnet structure depends on the lateral symmetry of the wave functions. This symmetry-filtering effect is converted into a large spin-filtering effect if the wave function with the preferred symmetry only exists in one of the two spin channels in the ferromagnetic electrodes. Such a spin-filtering effect was theoretically predicted to give rise to a very large tunneling magnetoresistance (TMR) in magnetic tunnel junctions (MTJs) such as Fe/MgO/Fe.[1,2]Indeed, a decade after the first successful demonstration of the room-temperature TMR effect,[3,4] giant TMR ratios up to 200% at RT were realized in Fe/MgO/Fe and CoFe/MgO/CoFe MTJs.[5,6] These TMR ratios in MgO-based junctions are much higher than those found in the Al_2O_3-based junctions, where the TMR is only about 40–80 %,[7–9] mainly limited by the disordered Al_2O_3 barrier. The giant leap of TMR has attracted a great deal of attention not only because of the MTJs broad applications in devices such as biosensors, hard-disk read heads, and magnetic random access memory[10–12] but also due to its important roles in fundamental research on electronic band structure, the Kondo effect, and spin-orbital interaction.[13–16]

Thermal annealing has proven to be one of the most crucial steps to achieve high TMR ratios.[17] It is during the post-annealing process that the TMR increases up to a few hundred percent, from typically 20–40 % in the as-prepared state. Particularly for CoFeB/MgO/CoFeB junctions, which are the most widely used system with the highest TMR among all the MTJs with MgO barrier,[18,19] the matching of the Bloch waves in the electrodes to the corresponding evanescent waves in the barrier only occurs after initially amorphous CoFeB layers crystallize in the (001) orientation during thermal annealing.[11,20] Unfortunately, compared to the extensive investigations on the effects of annealing temperature, the dependence of coherent tunneling on annealing time has largely been neglected.[18,21–23] Therefore, there was little understanding about the evolution of magnetoresistance during annealing in this important system. We have previously found that the crystallization of CoFeB occurs on a time scale of seconds and that the giant TMR quickly develops at the beginning of annealing.[24,25] However, many questions of fundamental importance are still not answered, such as what are the different dynamic behaviors of TMR under annealing at different temperatures? What is the exact physical origin for such behaviors? What are the different roles played by CoFeB and MgO? What is the feature for the onset of coherent tunneling in conductance?

In this paper, we attempt to address these questions. We report the first systematic study on the growth of symmetry-conserved tunneling during thermal annealing over a wide temperature range. The unique coherent tunneling properties in MgO junctions were exploited by varying the annealing time. The development of giant TMR during thermal annealing was shown to be qualitatively describable through an empirical model involving crystallization, defects reduction, and diffusion processes. More importantly, this model allows us to separate the different contributions of CoFeB and MgO to the development of giant coherent tunneling. The understanding of the physics governing the evolution of coherent tunneling, in turn, provides us with insights to optimize the MTJs for achieving better spintronics devices. We also notice there were studies in the past involved with annealing-time dependence of TMR in MTJs where noncoherent tunneling dominates.[26–28]

The MTJs in this paper were fabricated using a customized six-source sputtering system. The sample structures are Si/SiO2/Ta 7/Ru 20/Ta 7/CoFe 2/IrMn 15/CoFe 2/Ru 1.7/CoFeB 3/MgO (or Al_2O_3) 1.1–3.2/CoFeB 3/Ta 8/Ru 10 (numbers indicate layer thickness in nanometers). The base pressure of the sputtering chamber is 5×10^{-8} Torr. All the metal layers were deposited by dc sputtering under a pressure of 2 mTorr. The MgO layer was deposited by rf sputtering under a pressure of 1.2 mTorr. The deposition rate of MgO layer is set at 0.25 Å/s. The MTJ samples with the size of 5–100 μm were defined by the standard microfabrication procedures including multistep of photolithography,

 ©2010 The American Physical Society

ion-beam milling, and electrode deposition. In order to study the evolution of TMR in very short-time durations, the MTJs were annealed in a rapid thermal anneal system, in a pure Ar atmosphere for temperatures up to 500 °C. The transport measurement was performed in the four-probe configuration on a probestation. The x-ray photoelectron spectroscopy (XPS) study was performed in a PHI 5600 XPS system using monochromatic Al $K\alpha$ x rays and a hemispherical electron detector set to a pass energy of 58.7 eV. More details about sample fabrication and testing techniques are described by our previous publications.[24,25,29]

The giant TMR in CoFeB/MgO/CoFeB junctions is developed through the so-called solid-state epitaxy process during annealing.[30,31] The MgO barrier fabricated by rf sputtering has a very strong (001) texture when deposited on the amorphous CoFeB bottom electrode. During the postgrowth thermal annealing, the top and bottom interfaces of the highly (001)-oriented MgO layer serve as templates for the crystallization of amorphous CoFeB layers in the (001) orientation, thus forming the out-of-plane epitaxial CoFeB(001)/MgO(001)/CoFeB(001) sandwich structure.[11,20] Therefore, the highly spin-polarized, slow-decaying Δ_1 band electrons gives rise to the giant TMR effect through the symmetry-conserved coherent tunneling.[1,2]

The most dramatic effect of annealing time in this study is seen in Fig. 1(a): the TMR $[G_{\mathrm{P}}/G_{\mathrm{AP}}-1$, where G_{P} and G_{AP} are the conductance in the parallel (P) and antiparallel (AP) states, respectively$]$ in the as-prepared junction is 25% whereas it increases to 250% with only 30 s annealing at 500 °C. The TMR further increases to 290% after 90 s annealing, attaining its maximum value at about 300 s and then starts decreasing for being annealed longer than 400 s. The resistance-area product (RA) for the parallel state before annealing is 250 KΩ μm^2 for this junction. The decrease in exchange pinning strength during annealing is most likely due to the deteriorated synthetic antiferromagnetic layers of CoFe/Ru/CoFeB, caused by the diffusion of Ru and/or Mn. Figure 1(b) summarizes the results for more than 500 MTJs tested in this study. The error bars designate the standard deviation of TMR for MTJs with MgO thickness ranging from 1.5 to 3 nm. Each junction was annealed successively for different durations of time at a specific temperature. Generally, the evolution of TMR consists of three distinct regions: a sharp increase in the first region at the beginning of annealing, a very gradual increase toward saturation in second region, and finally the decreasing of TMR in the third region after prolonged annealing. The third region where the TMR starts decreasing is more appreciable for annealing carried above 400 °C. This evolution of TMR under different annealing temperatures is replotted in the log scale as shown in Fig. 1(c) in order to reveal clearly the behaviors for annealing as short as a few seconds and as long as 250 h in the same graph. For applications such as hard-disk read-head and current-induced magnetization switching, moderate TMR of 150–200 % is sufficient.[32,33] The horizontal line in Fig. 1(c) marks the optimal annealing time to achieve 180% TMR under different temperatures. The time needed to achieve the same TMR ratio can differ by more than four orders of magnitude if the annealing temperature is changed by less than 50% (from 290 to 500 °C), demonstrating the strongly thermal-activated behavior as one would expect.

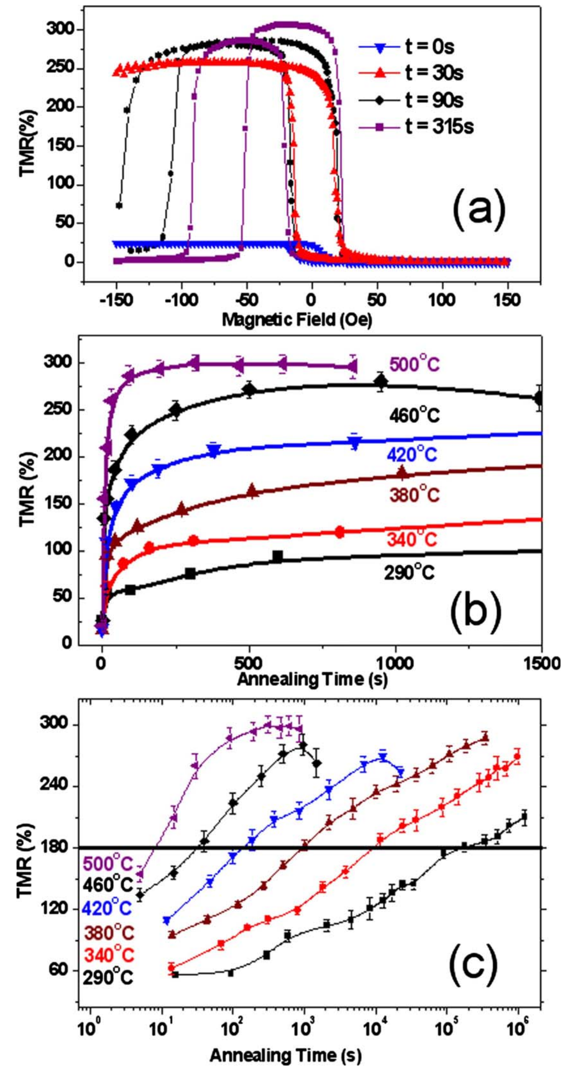

FIG. 1. (Color online) (a) TMR curves of the CoFeB/MgO/CoFeB junctions after annealing for different time durations at 500 °C. (b) The evolution of TMR at different temperatures on a linear scale. (b) Annealing-time dependence of TMR at different temperatures on a log scale. The horizontal line marks out the 180% TMR suitable for most applications.

The diffusion of Mn atoms into the MgO barrier during the annealing process is known to be detrimental to TMR. The Mn is exclusively used in the antiferromagnetic layer to provide the exchange pinning for the bottom electrodes of the tunneling junctions. The XPS study has been carried out to investigate the Mn content in the MgO barrier. The sample structure used was Si/SiO2/Ta 7/Ru 20/Ta 7/CoFe 2/IrMn 15/CoFe 2/Ru 1.7/CoFeB 3/MgO 2.5, with unit in nanometer. The Mn $2p$ core spectra for the as-prepared sample and annealed samples are shown in Fig. 2. For the as-prepared sample and the sample annealed for 4 min at 460 °C, the barrier shows no traces of Mn. The TMR is about 250% after being annealed for 4 min as shown in Fig. 1. Whereas after the annealing of 40 min at 460 °C, the Mn $2p$ core spectrum is clearly showing up in the barrier, directly resulting in the decrease in TMR as discussed later.

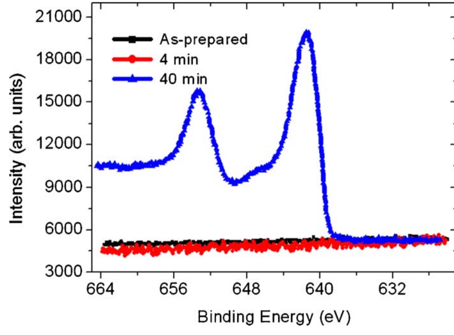

FIG. 2. (Color online) Mn $2p$ core spectra detected in the MgO barrier layer. The annealing temperature is 460 °C.

These results demonstrate that the annealing time to achieve best TMR need to be carefully chosen to maximize the coherent tunneling and minimize the diffusion of Mn. The highest reported TMR value in single-barrier MTJs with exchange pinning layers is around 360%,[22] mainly limited by Mn diffusion induced by long annealing. The highest TMR of 310% in our study was achieved in MTJs annealed for 5 min at 500 °C, indicating that one could possibly achieve a larger TMR by annealing at a higher temperature for a shorter time.

The annealing-time dependence of G_P and G_{AP} at 420 °C in a junction with a 3 nm MgO barrier (*RA* for the parallel state before annealing is 300 MΩ μm^2) is shown in Fig. 3(a). In sharp contrast to Al_2O_3-based junctions as to be discussed next, G_P and G_{AP} in the MgO junctions behave very differently: the G_P quickly increases at the early stages of annealing and then starts slowly decaying after being annealed for longer than 7 min. Meanwhile, G_{AP} drops about 25% after 7 min annealing, followed by a similar slow decrease. It is known that several processes are simultaneously occurring during the annealing, including the crystallization of amorphous CoFeB, reduction in defects (vacancies, interstitials, and grain boundaries, etc.) in the MgO barrier, and the diffusion of impurities such as B, Ru, or Mn (even Ta after long period of annealing[18]) into the barrier. The heretofore unobserved sharp increase in G_P is the direct consequence for the onset of spin-filtering coherent tunneling through the highly conducting Δ_1 band electrons from the CoFeB(001)/MgO(001) interfaces as predicted by the theory,[1] which is absent in the Al_2O_3 junctions. The decrease in G_P after about 7 min indicates that diffusion becomes appreciable at this time, as any extrinsic impurity scattering centers will perturb the lowest decay channel and increase the resistance.[1,34,35] The TMR value corresponding to the turning point of G_P is 190% as shown in Fig. 3(b). This discovery immediately shows that the annealing time should be carefully chosen for applications such as magnetic read head where minimal *RA* and a moderate TMR are highly desired.

The magnetoresistance in Al_2O_3-based MTJs were often described by the classic Julliere model.[36] However, the Julliere model cannot be applied here to the giant TMR arising from coherent tunneling of Bloch electrons in CoFeB(001)/MgO(001)/CoFeB(001) junctions.[11] More generally, the TMR is determined by the different transmission probabilities in parallel and antiparallel states, instead of by the spin polarization of bulk materials. The conductance of the tunnel junction can be expressed in the Landauer formalism as[1,37]

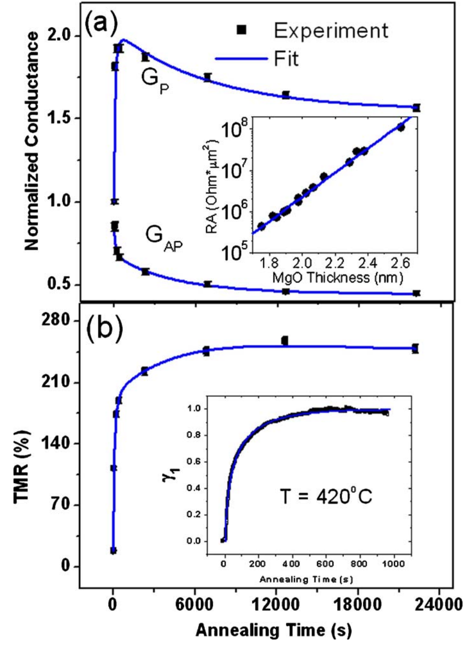

FIG. 3. (Color online) (a) Annealing-time dependence of G_P and G_{AP} for the MgO junction annealed at 420 °C. Lines are the fittings to Eq. (2). Inset shows the determination of κ_0 by WKB approximation. (b) Annealing-time dependence of TMR at 420 °C. The solid line is the fitting according to Eq. (2). Inset shows the time dependence of the crystalline fraction of CoFeB determined by the *in situ* diffraction. The solid line is the fit to the JMA model.

$$G = \frac{e^2}{h} \sum_{k_\parallel, k_\parallel'} [T^{++}(k_\parallel, k_\parallel')]_{E_F}, \tag{1}$$

where $T^{++}(k_\parallel, k_\parallel')$ is the transmission probability and $k_\parallel, k_\parallel'$ denote Bloch states in the bottom and top electrodes, and $k_\parallel = k_\parallel'$ when we consider that the electrode/barrier interfaces are translationally invariant. Note the $k_\parallel = k_\parallel'$ approximation only applies to the epitaxial MgO barrier because the scattering is mostly diffusive in junction with an amorphous Al_2O_3 barrier due to disorder. If we assume the total transmission coefficient after integration over the $k_\parallel$ space in a thick barrier MTJ can be represented by the product of two contributions from electrodes and barrier, respectively, we can write the conductance in the P and AP states as

$$G_{P,AP} \propto \frac{e^2}{h} [T_1^{P,AP} \gamma_1 + T_2^{P,AP} \gamma_2] e^{-d[\kappa_0 + \kappa^{P,AP} \phi(t)]}. \tag{2}$$

The term in the bracket is the contribution from the electrodes, where $T_1^{P,AP}$ and $T_2^{P,AP}$ are the fitting parameters for crystalline and amorphous parts of CoFeB, $\gamma_1(t)$ and $\gamma_2(t)$, respectively. The exponential term stands for the contribution from the barrier, where d is the MgO thickness and κ_0 is decay rate of the evanescent wave in the as-prepared junction. The decay rate is primarily determined by the band structure and the lowest decay rate in MgO belongs to these

electrons with Δ_1 symmetry. Compared to the drastic structural change in CoFeB, the MgO only undergoes minor structural modification as revealed previously,[24,25] implying the electronic band structure of MgO is not greatly changed if the annealing is not too long. The defect reduction in MgO will lower the decay rate due to the reduction in scattering for the electrons having high symmetry and the diffusion will increase the decay rate on the other hand. It was reported that the time dependence of the defect density in a thin film during annealing follows $N(t) \propto N_0 e^{-t/\alpha}$,[38] and the concentration of the diffused atoms into the neighboring thin film in a multilayer system follows $C(t) \propto -C_0 e^{-t/\beta}$,[39] where N_0, C_0, α, and β are parameters depending on the material and temperature. However, the experimental determination of the time-resolved defects density and exact concentration of impurity species such as B or Ru in an ultrathin MgO film remains very challenging. Hence in the current model, these two effects cannot be explicitly separated. The change in decay rates in the complex energy band of MgO due to the combination of these two effects is approximated by $\kappa^{\mathrm{P,AP}}\phi(t)$, where $\kappa^{\mathrm{P,AP}}$ are constants, $\phi(t) = 1 - e^{-t/t_0^{\mathrm{P,AP}}}$ and $t_0^{\mathrm{P,AP}}$ are parameters obeying the Arrhenius equation. In a few very recent experiments, the Boron concentration in the MgO layer was probed by electron energy-loss spectroscopy.[40,41] The activation energy for the diffusion of B into MgO was determined as 1.3 eV in one of the experiments.[40] The MgO monitor layer used was 25 nm thick and the distribution of Boron atoms in MgO followed a complementary error-function characteristic. It is known that the error-function distribution is more likely to be valid for a semi-infinite media. The real situation in a 1–3-nm-thick MgO barrier could be quite different. The distribution is a complex function with both sinusoidal and exponential terms instead.[42] The accurate determination of the interdiffusion in this system could perhaps be achievable through the small-angle x-ray diffraction[39] in future experiments.

In order to describe the time dependence of TMR, it is critical to determine $\gamma_1(t)$, the exact amount of CoFeB in crystalline form at any given time [after that $\gamma_2(t)$ is also known since $\gamma_1(t) + \gamma_2(t) = 1$]. We have characterized the crystallization rate of CoFeB by the *in situ* synchrotron-based x-ray diffraction at beamline X-20 C of the National Synchrotron Light Source.[25] Unpatterned MTJs samples without underlayers on glass substrate were used to avoid the diffraction peaks from the buffer layers and Si wafer, which interferes with CoFe (002) peak. The structure of the films is CoFeB 6 nm/MgO 10 nm/CoFeB 6 nm/Ta 5 nm. The volume fraction of the crystallized CoFeB during annealing at 420 °C is shown in the inset of Fig. 3(b). The nucleation and growth of a crystalline material from its amorphous phase during annealing can be described by the Johnson-Mehl-Avrami (JMA) model,[43,44]

$$\gamma_1(t) = 1 - \exp\{-[K(t-\tau)]^n\}, \quad (3)$$

where n is a constant dependent on the nucleation and growth rate, τ is the incubation time, and K is defined by the Arrhenius equation as $K = K_0 e^{-E_a/RT}$ with constant K_0 and the effective activation energy E_a for the amorphous to crystalline transition. The volume fraction of the crystalline percentage of CoFeB can be well fit by the JMA equation as shown in the inset of Fig. 3(b). The best-fitted values for K, n, and τ are 0.015 s^{-1}, 0.6, and 6.6 s, respectively.

Once the crystallization rate of CoFeB is determined, Eq. (2) can be used to fit the normalized G_P and G_AP with $\kappa_0 = 8.6\ \mathrm{nm}^{-1}$ determined by the WKB approximation as shown in the inset of Fig. 3(a). The evolution of both G_P and G_AP can be well fitted to this model as shown by the solid lines of Fig. 3(a). The change in decay rates in P and AP states during annealing were determined to be 0.10 nm^{-1} and 0.14 nm^{-1}, respectively. It is interesting to note that the TMR still increases even though G_P starts to decrease after the turning point and that G_P seems to decrease faster than G_AP. The reason might be that conductance in the P state being very sensitive to the impurity scattering as theoretically predicted.[1,34] However, this drop of G_P is overbalanced by the decrease in G_AP where the effect of defect reduction dominates so that the conduction of Δ_5 and $\Delta_{2'}$ band electrons is further reduced due to the improvement of the barrier structure. Therefore, the TMR, as the result of the competition, keeps increasing as long as $\Delta G_\mathrm{P}/G_\mathrm{P} > \Delta G_\mathrm{AP}/G_\mathrm{AP}$ is satisfied. Once the behaviors of G_P and G_AP are understood, the TMR ratio now can be readily calculated. As shown in Fig. 3(b), the calculated TMR curve agrees very well with the experimental results.

More importantly, this model allows us to look into the different contributions from CoFeB and MgO during the evolution of TMR. Figure 4(a) shows the simulated TMR

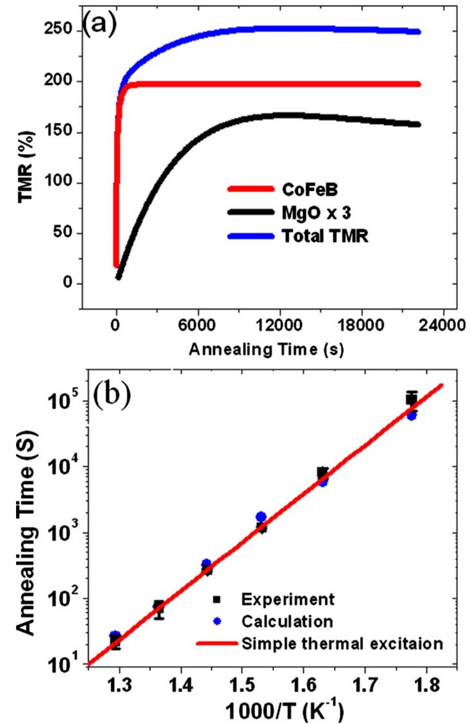

FIG. 4. (Color online) (a) Simulated TMR curve and the different contributions from CoFeB and MgO. Note the contribution of MgO is multiplied by 3 in order to show details. (b) Experimental and calculated annealing time needed to achieve 180% TMR at different temperatures. An activation energy of 140 KJ/mol is yielded from the slope of linear fitting.

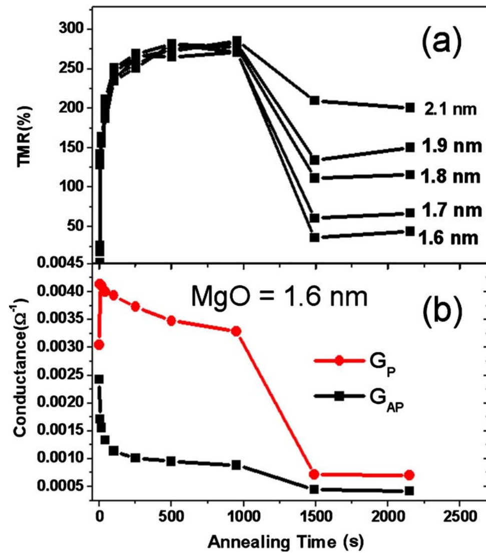

FIG. 5. (Color online) (a) Failure behaviors for MTJs with different barrier thicknesses at 460 °C. (b) The time dependence of conductance for the MTJ with 1.6 nm MgO barrier.

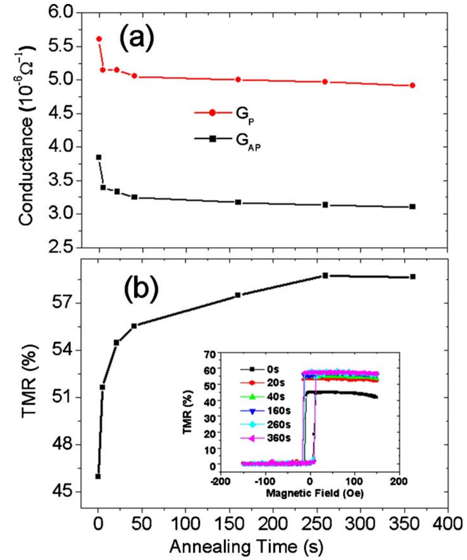

FIG. 6. (Color online) (a) The annealing-time-dependent parallel and antiparallel conductance in the Al_2O_3 junctions with barrier thickness of 3.3 nm. The annealing temperature is 340 °C. (b) The corresponding evolution of TMR. The inset shows the TMR curves after different annealing-time durations for the same junction.

curve using the parameters obtained in the fitting by Eq. (2). Now the physical mechanisms for the three distinct regions of the evolution of TMR are clearly revealed. The quick increase in TMR in the first region is mostly due to the fast crystallization of CoFeB. The slow increase in TMR in the second region, which starts at the turning point of G_P as shown in Fig. 4(a), is mostly due to the contribution from the MgO barrier. Lastly, the drop of TMR in the third region is caused by the reduced transmission of MgO due to increased diffusion at prolonged annealing. Furthermore, the time needed to achieve a certain TMR ratio in the first region can also be estimated by only considering the activation of CoFeB using the terms in the bracket of Eq. (2). The experimental and calculated time for achieving 180% TMR under different temperatures is shown in Fig. 4(b). The activation energy of 150 KJ/mol for the crystallization process is used as determined previously through the synchrotron-based x-ray diffraction.[25] One could also fit the experimental values with a simple thermally activated Arrhenius-type equation ($t \sim e^{E_a/RT}$). The slope of this fitting yields the activation energy of 140 KJ/mol, a value very close to the activation energy of CoFeB. Therefore, the comprehensive behaviors during the development of the coherent tunneling can be qualitatively understood by our model.

After a longer period of annealing at high temperatures, in most cases the TMR will decrease abruptly at a certain time. Such failure behaviors are shown in Fig. 5(a) for the annealing at 460 °C. This sudden drop of TMR is caused by the abrupt decrease in G_P presented in Fig. 5(b), indicating that the high conductance coherent channel is seriously disturbed by impurity scattering. This probably occurs when the Mn atoms diffused from the deep layer reaches a critical concentration, which drastically alters the electronic band structure of MgO, thus beyond the scope of our current model. Nevertheless, it is worth mentioning that the TMR in the junctions with thinner barriers drops much faster, which again demonstrates that careful determination of annealing time is vital to avoid "overannealing" the MTJs, especially in the case when a very thin layer of MgO barrier is needed for the spin-transfer torque experiments.[32,33]

For comparison, the evolution of TMR during annealing for the MTJs with Al_2O_3 barriers was also investigated. Previously it was reported that the TMR in Al_2O_3 junctions can be enhanced by rapid thermal anneal. The barrier width and barrier height fitted from Simmon's model showed abrupt changes at the beginning of annealing.[26] The explicit dependence of magnetoresistance on annealing time was not reported. Figure 6 shows the annealing-time dependence of G_P and G_{AP} in a junction with 3.3 nm of Al_2O_3 barrier (RA for the parallel state before annealing is 1760 MΩ μm^2). Both G_P and G_{AP} decrease sharply at the beginning then stay almost flat in the rest of annealing. The decreasing rate of G_P is larger than G_{AP}. As a result, the TMR increases from 46% in the as-prepared state to 59% after being annealed for 360 s at 340 °C. These changes in conductance and TMR were previously attributed to the redistribution of oxygen in the Al_2O_3 barrier and reduction in roughness at the interfaces.[17,26] Further annealing beyond 360 s will result in the decrease in TMR. The MgO-based junctions, as presented in Fig. 1(c), show no sign of decreasing even after hundreds of hours of annealing at 340 °C, demonstrating the superior thermal stability of MgO over Al_2O_3.

In conclusion, we have systematically studied the evolution of symmetry-conserved tunneling during annealing in CoFeB/MgO/CoFeB junctions. The optimal annealing time for different temperature was determined. The tunneling conductance in the parallel state exhibits a novel behavior due to the onset of coherent tunneling of Δ_1 Bloch electrons. The evolution of TMR consists of three distinct regions, caused by different contributions from CoFeB electrodes and the

MgO barrier. These behaviors of coherent tunneling can be qualitatively understood through an empirical model based on the Landauer tunneling picture.

The authors are grateful to Brian Kirby and Kathryn Krycka for stimulating discussion on the crystallization experiment. This work at Delaware was supported by DOE under Grant No. DE-FG02-07ER46374 and NSF under Grant No. DMR0827249. The work at MIT was supported by NSF under Grant No. DMR0504158 and ONR under Grant No. N00014-09-1-0177. Use of the National Synchrotron Light Source, Brookhaven National Laboratory, was supported by the U.S. Department of Energy, Office of Science, Office of Basic Energy Sciences, under contract No. DE-AC02-98CH10886.

*Present address: Department of Physics and Astronomy, Johns Hopkins University; wgwang@pha.jhu.edu

†jqx@udel.edu

[1] W. H. Butler, X.-G. Zhang, T. C. Schulthess, and J. M. MacLaren, Phys. Rev. B **63**, 054416 (2001).

[2] J. Mathon and A. Umerski, Phys. Rev. B **63**, 220403(R) (2001).

[3] J. S. Moodera, L. R. Kinder, T. M. Wong, and R. Meservey, Phys. Rev. Lett. **74**, 3273 (1995).

[4] T. Miyazaki and N. Tezuka, J. Magn. Magn. Mater. **139**, L231 (1995).

[5] S. Yuasa, T. Nagahama, A. Fukushima, Y. Suzuki, and K. Ando, Nature Mater. **3**, 868 (2004).

[6] S. S. P. Parkin, C. Kaiser, A. Panchula, P. M. Rice, B. Hughes, M. Samant, and S. H. Yang, Nature Mater. **3**, 862 (2004).

[7] H. X. Wei, Q. H. Qin, M. Ma, R. Sharif, and X. F. Han, J. Appl. Phys. **101**, 09B501 (2007).

[8] D. X. Wang, C. Nordman, J. M. Daughton, Z. H. Qian, and J. Fink, IEEE Trans. Magn. **40**, 2269 (2004).

[9] L. Gao, X. Jiang, S.-H. Yang, P. M. Rice, T. Topuria, and S. S. P. Parkin, Phys. Rev. Lett. **102**, 247205 (2009).

[10] W. Shen, B. D. Schrag, M. J. Carter, and G. Xiao, Appl. Phys. Lett. **93**, 033903 (2008).

[11] S. Yuasa and D. D. Djayaprawira, J. Phys. D **40**, R337 (2007).

[12] W. J. Gallagher and S. S. P. Parkin, IBM J. Res. Dev. **50**, 5 (2006).

[13] K. I. Lee, S. J. Joo, J. H. Lee, K. Rhie, T. S. Kim, W. Y. Lee, K. H. Shin, B. C. Lee, P. LeClair, J. S. Lee, and J. H. Park, Phys. Rev. Lett. **98**, 107202 (2007).

[14] H. Saito, S. Yuasa, and K. Ando, Phys. Rev. Lett. **95**, 086604 (2005).

[15] M. Bowen, A. Barthelemy, M. Bibes, E. Jacquet, J.-P. Contour, A. Fert, F. Ciccacci, L. Duò, and R. Bertacco, Phys. Rev. Lett. **95**, 137203 (2005).

[16] L. Gao, X. Jiang, S.-H. Yang, J. D. Burton, E. Y. Tsymbal, and S. S. P. Parkin, Phys. Rev. Lett. **99**, 226602 (2007).

[17] R. C. Sousa, J. J. Sun, V. Soares, P. P. Freitas, A. Kling, M. F. da Silva, and J. C. Soares, Appl. Phys. Lett. **73**, 3288 (1998).

[18] S. Ikeda, J. Hayakawa, Y. Ashizawa, Y. M. Lee, K. Miura, H. Hasegawa, M. Tsunoda, F. Matsukura, and H. Ohno, Appl. Phys. Lett. **93**, 082508 (2008).

[19] L. X. Jiang, H. Naganuma, M. Oogane, and Y. Ando, Appl. Phys. Express **2**, 083002 (2009).

[20] Y. S. Choi, K. Tsunekawa, Y. Nagamine, and D. Djayaprawira, J. Appl. Phys. **101**, 013907 (2007).

[21] D. D. Djayaprawira, K. Tsunekawa, M. Nagai, H. Maehara, S. Yamagata, N. Watanabe, S. Yuasa, Y. Suzuki, and K. Ando, Appl. Phys. Lett. **86**, 092502 (2005).

[22] Y. M. Lee, J. Hayakawa, S. Ikeda, F. Matsukura, and H. Ohno, Appl. Phys. Lett. **89**, 042506 (2006).

[23] Y. S. Choi, Y. Nagamine, K. Tsunekawa, H. Maehara, D. D. Djayaprawira, S. Yuasa, and K. Ando, Appl. Phys. Lett. **90**, 012505 (2007).

[24] W. G. Wang, C. Ni, A. Rumaiz, Y. Wang, X. Fan, T. Moriyama, R. Cao, Q. Y. Wen, H. W. Zhang, and J. Q. Xiao, Appl. Phys. Lett. **92**, 152501 (2008).

[25] W. G. Wang, J. Jordan-sweet, G. X. Miao, C. Ni, A. Rumaiz, L. Shah, X. Fan, P. Parson, R. Stearrett, R. Nowak, J. S. Moodera, and J. Q. Xiao, Appl. Phys. Lett. **95**, 242501 (2009).

[26] K. I. Lee, J. H. Lee, W. Y. Lee, K. W. Rhie, J. G. Ha, C. S. Kim, and K. H. Shin, J. Magn. Magn. Mater. **239**, 120 (2002).

[27] P. W. T. Pong, M. Schmoueli, F. Li, and W. F. Egelhoff, J. Appl. Phys. **103**, 07E937 (2008).

[28] H.-C. Chung and S.-R. Lee, J. Appl. Phys. **103**, 07A914 (2008).

[29] Y. Z. Liu, W. G. Wang, T. Moriyama, J. Q. Xiao, and Z. Zhang, Phys. Rev. B **75**, 134420 (2007).

[30] M. von Allmen, S. S. Lau, J. W. Mayer, and W. F. Tseng, Appl. Phys. Lett. **35**, 280 (1979).

[31] S. S. Lau, J. Vac. Sci. Technol. **15**, 1656 (1978).

[32] J. A. Katine and E. E. Fullerton, J. Magn. Magn. Mater. **320**, 1217 (2008).

[33] J. Z. Sun and D. C. Ralph, J. Magn. Magn. Mater. **320**, 1227 (2008).

[34] J. P. Velev, K. D. Belashchenko, S. S. Jaswal, and E. Y. Tsymbal, Appl. Phys. Lett. **90**, 072502 (2007).

[35] G. X. Miao, Y. J. Park, J. S. Moodera, M. Seibt, G. Eilers, and M. Munzenberg, Phys. Rev. Lett. **100**, 246803 (2008).

[36] M. Julliere, Phys. Lett. A **54**, 225 (1975).

[37] R. Landauer, Philos. Mag. **21**, 863 (1970).

[38] V. Vand, Proc. Phys. Soc. London **55**, 222 (1943).

[39] H. E. Cook and J. E. Hilliard, J. Appl. Phys. **40**, 2191 (1969).

[40] S. S. Mukherjee, D. MacMahon, F. Bai, C.-L. Lee, and S. K. Kurinec, Appl. Phys. Lett. **94**, 082110 (2009).

[41] J. J. Cha, J. C. Read, W. F. Egelhoff, P. Y. Huang, H. W. Tseng, Y. Li, R. A. Buhrman, and D. A. Muller, Appl. Phys. Lett. **95**, 032506 (2009).

[42] J. Crank, *The Mathematics of Diffusion* (Oxford University Press, New York, 1975).

[43] M. Avrami, J. Chem. Phys. **9**, 177 (1941).

[44] J. Z. Jiang, Y. X. Zhuang, H. Rasmussen, J. Saida, and A. Inoue, Phys. Rev. B **64**, 094208 (2001).